IOPscience iopscience.iop.org

Home Search Collections Journals About Contact us My IOPscience

Influence of RF-sputtering power on formation of vertically stacked $Si_{1-x}Ge_x$ nanocrystals between ultra-thin amorphous Al_2O_3 layers: structural and photoluminescence properties

This article has been downloaded from IOPscience. Please scroll down to see the full text article.

2013 J. Phys. D: Appl. Phys. 46 385301

(http://iopscience.iop.org/0022-3727/46/38/385301)

View the table of contents for this issue, or go to the journal homepage for more

Download details:
IP Address: 193.137.16.114
The article was downloaded on 05/09/2013 at 22:50

Please note that terms and conditions apply.

J. Phys. D: Appl. Phys. **46** (2013) 385301 (10pp) doi:10.1088/0022-3727/46/38/385301

Influence of RF-sputtering power on formation of vertically stacked $Si_{1-x}Ge_x$ nanocrystals between ultra-thin amorphous Al_2O_3 layers: structural and photoluminescence properties

E M F Vieira[1], J Martín-Sánchez[2,12], M A Roldan[3], M Varela[3,4], M Buljan[5], S Bernstorff[6], N P Barradas[7], N Franco[8], M R Correia[9], A G Rolo[1], S J Pennycook[4], S I Molina[10], E Alves[8], A Chahboun[1,11] and M J M Gomes[1]

[1] University of Minho, Centre of Physics and Physics Department, 4710-057 Braga, Portugal
[2] Laser Processing Group, Instituto de Óptica, CSIC, C/ Serrano 121, 28006 Madrid, Spain
[3] Universidad Complutense de Madrid, Departamento de Fisica Aplicada III, Madrid 28040, Spain
[4] Materials Science and Technology Division, Oak Ridge National Laboratory, Oak Ridge, TN 37831, USA
[5] Ruđer Bošković Institute, Bijenička cesta 54, Zagreb 10000, Croatia
[6] Elettra-Sincrotrone Trieste, SS 14 km163, 5, Basovizza 34149, Italy
[7] Universidade de Lisboa, Centro de Ciências e Tecnologias Nucleares, Instituto Superior Técnico, E.N. 10 (km 139,7), 2695-066 Bobadela LRS, Portugal
[8] Universidade de Lisboa, Instituto de Plasmas e Fusão Nuclear, Instituto Superior Técnico, Av. Rovisco Pais, 1049-001 Lisboa, Portugal
[9] University of Aveiro, Department of Physics and I3N, Campus Universitário de Santiago, 3810-193 Aveiro, Portugal
[10] Universidad de Cádiz, Departamento de Ciencia de los Materiales e Ing. Metalúrgica y Q. I., Cádiz, Spain
[11] FST Tanger, Physics Department, BP 416 Tanger, Morocco

E-mail: eliana_vieira@fisica.uminho.pt and mjesus@fisica.uminho.pt

Received 3 May 2013, in final form 22 July 2013
Published 4 September 2013
Online at stacks.iop.org/JPhysD/46/385301

Abstract
In this work, we investigate the structural and photoluminescence (PL) properties of $(SiGe+Al_2O_3)/Al_2O_3$ multi-layer films with layer thicknesses in the range of a few nanometres. The films were prepared by magnetron sputtering deposition at room temperature followed by an annealing process to promote the formation of small SiGe nanocrystals (NCs) (∼3 to 5 nm) embedded between ultra-thin (∼6 nm thickness) Al_2O_3 layers. Our results show that the structural and compositional properties of the films can be tuned by changing the RF-power. It is found that nearly spherical and well confined isolated SiGe NCs (∼5 nm) are obtained for an RF-power value of 80 W. The PL properties of the films were studied and optical emission in the blue visible wavelength region was observed.

(Some figures may appear in colour only in the online journal)

1. Introduction

The fabrication of nanostructures with dimensions below 100 nm and organized within large macroscopic areas is a prerequisite for many applications in the field of nanotechnology. In recent years, growing attention has been paid to semiconductor nanocrystals (NCs)/dielectric multi-layered systems because of their interesting size-tunable properties. This makes them suitable for applications in electronics, optoelectronics and solar cells [1–8]. For these

[12] Present address: Johannes Kepler University, Institute of Semiconductor and Solid State Physics, Altenbergerstrasse 69, 4040 Linz, Austria.

 © 2013 IOP Publishing Ltd Printed in the UK & the USA

applications, the morphological and structural properties of the NCs need to be precisely controlled in order to obtain high-quality multi-layers. For optimal performance, it is highly desirable to develop a fabrication method that allows one to obtain stable layers with low interfacial roughness, low inter-diffusion between layers and a high spatial density of NCs with homogeneous sizes in a very thin and well-defined two-dimensional layer, where the distance between adjacent NC layers can be maintained constant over large areas are also required.

A significant amount of research has been done on the preparation of high-quality multi-layer semiconductor films by different techniques, such as molecular beam epitaxy (MBE) [9], low-pressure chemical vapour deposition (LPCVD) [3], magnetron sputtering [2, 5, 6, 10] and magnetron sputtering combined with ion beam irradiation [11]. In particular, magnetron sputtering has been proved to be a useful, cheap and easy technique with less energy consumption for the fabrication of semiconductor NCs embedded in the dielectric oxide matrices of multi-functional films, where NCs show very strong confinement, electroluminescence, PL, non-linear refraction index and excellent charge trapping capabilities, among other functionalities [5, 12–14]. In thick semiconductor-material-rich oxide layers, the NC nucleation process takes place by means of a bulk diffusion mechanism where semiconductor atoms are supplied from all directions in the film during annealing. However, in thin nanometre-thick layers, a constrained two-dimensional diffusion process occurs and the size of semiconductor NCs is mainly conditioned by the layer thickness. In such cases it is expected that the resulting structures will be homogeneously distributed within a dielectric matrix. In fact, we have recently reported a stable multi-layer structure with the formation of well-organized SiGe NCs confined between 5 nm thick SiO_2 layers [10].

Alumina-based materials are very suitable for use in nanotechnology applications, due to their hardness, good mechanical strength, high stiffness and high dielectric constant, which provide much better gate properties in memory applications than more commonly used SiO_2 [15]. Although there are many studies about semiconductor NCs (Ge, Si or SiGe) embedded in SiO_2 multi-layer films, there are fewer reports about films where the embedding oxide matrix is Al_2O_3 [4, 16]. The light emission mechanism from Si/Ge NCs has been discussed extensively and attributed either to radiative recombination of quantum-confined states [17–20] or to defects at the NC/matrix interface or in the matrix itself [18, 20–22]. However, the mechanism of luminescence from Si/Ge NCs in the visible region is still unclear.

In the present work, $(SiGe+Al_2O_3)/Al_2O_3$ multi-layer structures with ultra-thin Al_2O_3 barrier layers (∼6 nm) prepared by RF-sputtering at room-temperature (RT) were investigated. The effect of the RF-power used in the deposition process on their structural, compositional and PL properties is discussed.

2. Experimental

2.1. Sample fabrication

$(SiGe+Al_2O_3)/Al_2O_3$ multi-layered stacks of 20 periods were fabricated at RT on p-type Si (1 0 0) substrates using a commercial RF-magnetron sputtering system (Alcatel SCM650 machine). The structures were grown by depositing alternating $SiGe+Al_2O_3$ and Al_2O_3 thin layers using a composite target consisting of an Al_2O_3 (99.999% purity) plate with several polycrystalline Si and Ge pieces resting on its surface and a pure Al_2O_3 target, respectively. The surface area ratio of the Si and Ge pieces on the Al_2O_3 target was 1 : 2. The sputtering system allowed automatic control of the movement of the sample-holder disc, the time it was in position for each sputtering (or pre-sputtering) treatment, as well as the sputtering working gas (4×10^{-3} mbar of Ar pressure). The residual pressure was 1×10^{-6} mbar. Two kinds of samples were fabricated by using different values of RF-power: 60 W (hereafter, film A) and 80 W (hereafter, film B). The deposition rates for film A were found to be 4.4 nm min^{-1} and 1.3 nm min^{-1}, for $SiGe+Al_2O_3$ and Al_2O_3 layers, respectively. For film B, the deposition rates were 5.4 nm min^{-1} and 1.8 nm min^{-1} approximately for $SiGe+Al_2O_3$ and Al_2O_3 layers, respectively. The nominal thicknesses of the layers were kept constant (4 nm of $SiGe+Al_2O_3$ and 6 nm of Al_2O_3). A top 6 nm thick Al_2O_3 capping layer was deposited in order to prevent Si and Ge atoms diffusing out from the top layer as much as possible. In order to obtain self-assembled SiGe NCs, the films were subjected to a two-step thermal treatment by combining conventional furnace and rapid thermal annealing (RTA) in a nitrogen atmosphere (6 mbar): (i) pre-annealing, using a conventional furnace at 800 °C for 10 min, to promote slow diffusion of the Si and Ge species within and along the SiGe rich-layers and to facilitate the self-assembly of SiGe clusters; (ii) RTA at 900 °C for 30 s for crystallization of SiGe clusters. In order to study the influence of the annealing temperature on the PL properties, one additional annealed sample was also prepared at 700 °C for 10 min (in a conventional furnace) followed by the RTA treatment at 900 °C for 30 s.

2.2. Experimental characterization

High-angle annular dark field (HAADF) images were recorded using an aberration corrected NION UltraSTEM200 scanning transmission electron microscope (STEM), operating at 200 kV, equipped with a Gatan Enfinium electron energy loss spectrometer (EELS). Cross-sectional samples were prepared using conventional methods: grinding and ion milling. Grazing incidence small angle x-ray scattering (GISAXS) measurements were performed at the SAXS beamline of the Elettra Synchrotron using a photon energy of 8 keV and several grazing incidence angles slightly above the critical angle of total external reflection. Low angle x-ray reflectometry (XRR) experiments were done using the Bruker-AXS D8 Discover diffractometer in symmetric geometry (Bragg–Brentano), using the Cu Kα_1 1.54 Å line collimated with a Göbel mirror, a two-bounce Ge(2 2 0) monochromator

and a 0.2 × 10 mm^2 primary slit. The investigated area on the sample was ∼10 × 10 mm^2. Rutherford backscattering spectroscopy (RBS) measurements were done using a 2.0 MeV $^4He^+$ ion beam impinging on the target at tilt angles up to 82° in order to obtain sufficient resolution to resolve the depth profile of the multi-layer structure at the nanometre scale. The scattering angle was 160°, with the detector located under the beam, in order to maximize the depth resolution at high tilt angles. Raman spectra were obtained at RT in a backscattering configuration with a Horiba Jobin Yvon LabRam HR800 UV spectrometer equipped with a CCD detector using the 325 nm excitation wavelength of the He–Cd laser line. The laser beam was focused on the surface of the sample with a beam spot size of about 0.8 μm. The PL spectra were recorded at RT using an UV laser (325 nm) for the PL excitations.

3. Results and discussion

3.1. Structural properties of the films: arrangement and size of NCs

Raman spectra for as-grown and annealed films A and B are shown in figure 1. Peaks at 521 cm^{-1} and 325 cm^{-1} arise from the crystalline Si substrate and the experimental setup, respectively. Only broad features corresponding to an amorphous phase are observed for as-grown films (figure 1(*a*)). After annealing (figure 1(*b*)) only film A exhibits three Raman peaks around 300, 400 and 500 cm^{-1} corresponding to Ge–Ge, Si–Ge and Si–Si vibrational modes of a crystalline SiGe alloy. The peaks have asymmetrical shapes and the Ge–Ge vibrational mode is blue-shifted with respect to the bulk material value (300.4 cm^{-1}). The observed shifts can be explained by the stress applied to the SiGe NCs by the Al_2O_3 matrix and/or the stress caused by the incorporation of Si. The absence of Raman features for the annealed film B can be explained by low Ge and Si concentrations in the film. This was confirmed by RBS analysis as shown below. Raman spectroscopy is a very useful technique for quantitative evaluation of the Ge content (x) and strain (ε) in SiGe alloy [23–25]. A Ge content (x) value of 0.60±0.05 in the $Si_{1-x}Ge_x$ alloy and a strain value of −0.025 ± 0.004 were calculated from the Raman spectrum for film A after annealing using the equations described in detail in [25].

Figure 2 shows HAADF-STEM images of films A and B after annealing. Intensities in HAADF images are approximately proportional to the square of the atomic number Z and hence, the distribution of NCs along the SiGe+Al_2O_3 film in a multi-layer structure can be well resolved. Atomic resolution images of crystalline $Si_{1-x}Ge_x$ NCs are presented for each film at the bottom of the figure where lattice fringes corresponding to {1 1 1} planes are observed. The corresponding lattice plane spacings for films A and B are 0.322 ± 0.003 nm (Ge (x) = 0.7) and 0.323 ± 0.003 nm (Ge (x) = 0.8), respectively. These values are between those corresponding to pure Si (0.314 nm) and Ge (0.327 nm) for the {1 1 1} family crystal planes, which indicates that the NCs formed are Ge-rich in good agreement with Raman observations within the experimental error. Averaged intensity

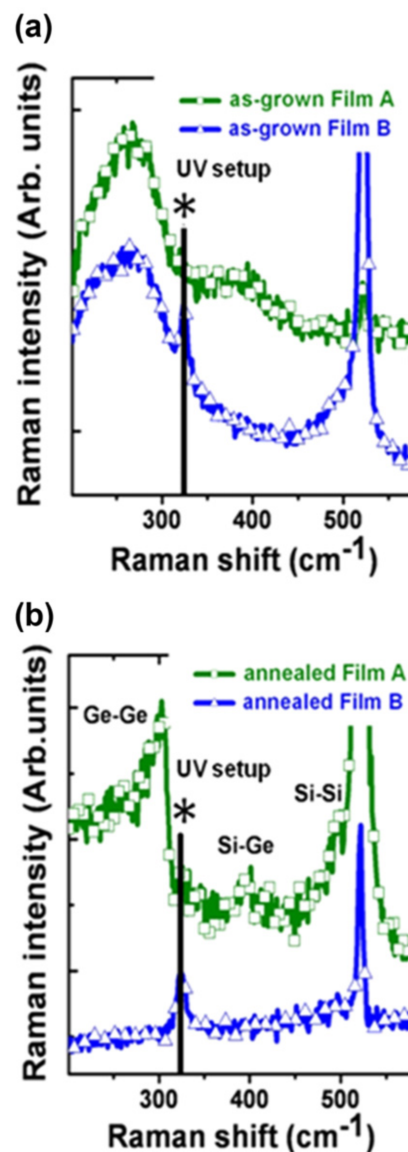

Figure 1. Raman spectra of as-grown (*a*) and annealed (*b*) films A and B. The peak at 325 cm^{-1} (*) comes from the UV experimental setup. A cross-polarized Raman spectrum for annealed film B has been obtained.

line profiles centred on the green arrow marked on these images were obtained after the application of a low-pass filter in Fourier space. Since Ge and Si have different Z numbers, the constituent atoms can be clearly identified.

We observe that after the annealing process, the layered structure remains with well-defined interfaces. The average period of these multi-layers is around 10 nm (thickness of Al_2O_3 is 6 nm) and the thickness of the whole structures is around 220 nm. For both samples, SiGe+Al_2O_3 and Al_2O_3 layers are well correlated to each other, but towards the surface the multi-layer starts to have a lateral oscillation. Positional degradation in the structural quality of multi-layer structures fabricated by magnetron sputtering deposition is well known [26]. A small intrinsic roughness in individual layers at the bottom of a multi-layer system leads to a large cumulative roughness towards the top of the multi-layer with the consequent degradation of the structure, as we have

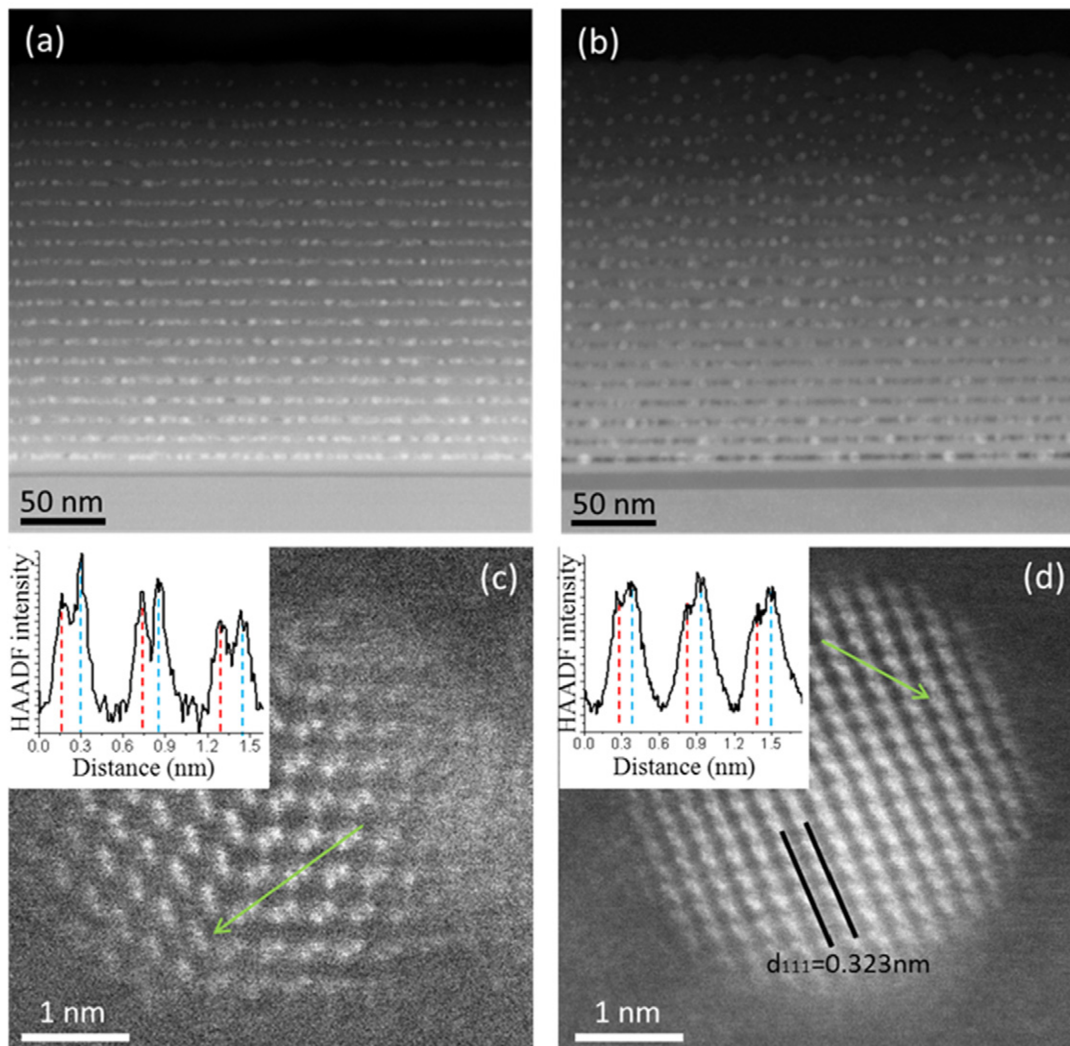

Figure 2. Low magnification cross-sectional HAADF-STEM images of the whole ML structure for annealed films A (*a*) and B (*b*). High-resolution HAADF-STEM images from films A (*c*) and B (*d*) of $Si_{1-x}Ge_x$ NCs, both taken from the bottom of the {1 1 1} SiGe lattice, where fringes are clearly visible. The dumbbells-type structure of the $Si_{1-x}Ge_x$ NCs is shown. Intensity trace along the green arrow drawn is reported, red dashed line points at the less bright atoms (Si), blue dashed line points at the brightest atoms (Ge).

recently demonstrated with SiGe/SiO_2 multi-layer structures [10]. However, it is interesting to note that this effect does not influence the confinement of the SiGe+Al_2O_3 layers. In particular, for film A, the HAADF image (figure 2(*a*)) reveals more continuous SiGe-rich layers with small clusters formed much closer to each other than in the case of film B (figure 2(*b*)). Nearly spherical confined NCs in the Al_2O_3 layers with a broader size distribution are observed in film A. The NCs are smaller (around 3.5 nm) in the top layers with respect to the bottom layers close to the substrate (around 5 nm). On the other hand, film B shows the formation of nearly spherical confined NCs, with a size of approximately 5 nm averaged throughout the whole structure. The arrangement and size distribution of the NCs formed in the annealed films can be explained in terms of the RF-power used in the deposition process, the substrate and film being subjected to a flux of energetic atoms originated in the sputtering event. This flux includes both sputtered atoms and energetic Ar neutrals that are reflected from the sputtering target in charge-exchange collisions. When an RF-power value of 60 W is used (film A), the as-grown films have been subjected to sputtered species of relatively low kinetic energy, which leads to a low surface mobility of adatoms and also a random size distribution of atoms and a weak propensity for atomic rearrangement. However, in films grown at an RF-power value of 80 W (film B), the sputtered species have a higher kinetic energy when arriving at the substrate, thus their mobilities are high enough to lead to a more uniform spatial distribution of the clusters within the layers. The results obtained show that after the annealing treatment, spherical NC formation is favoured for film B (80 W RF power) with a more uniform size distribution.

GISAXS was used to further investigate the structural properties of the films. This technique allows in-plane investigation of the layered film structure with depth resolution over large areas [16]. GISAXS maps of as-grown and annealed films for a grazing incidence beam angle greater than the critical angle ($\alpha > \alpha_{cr}$) are shown in figure 3. In the case of the as-grown films, Bragg sheets are resolved and

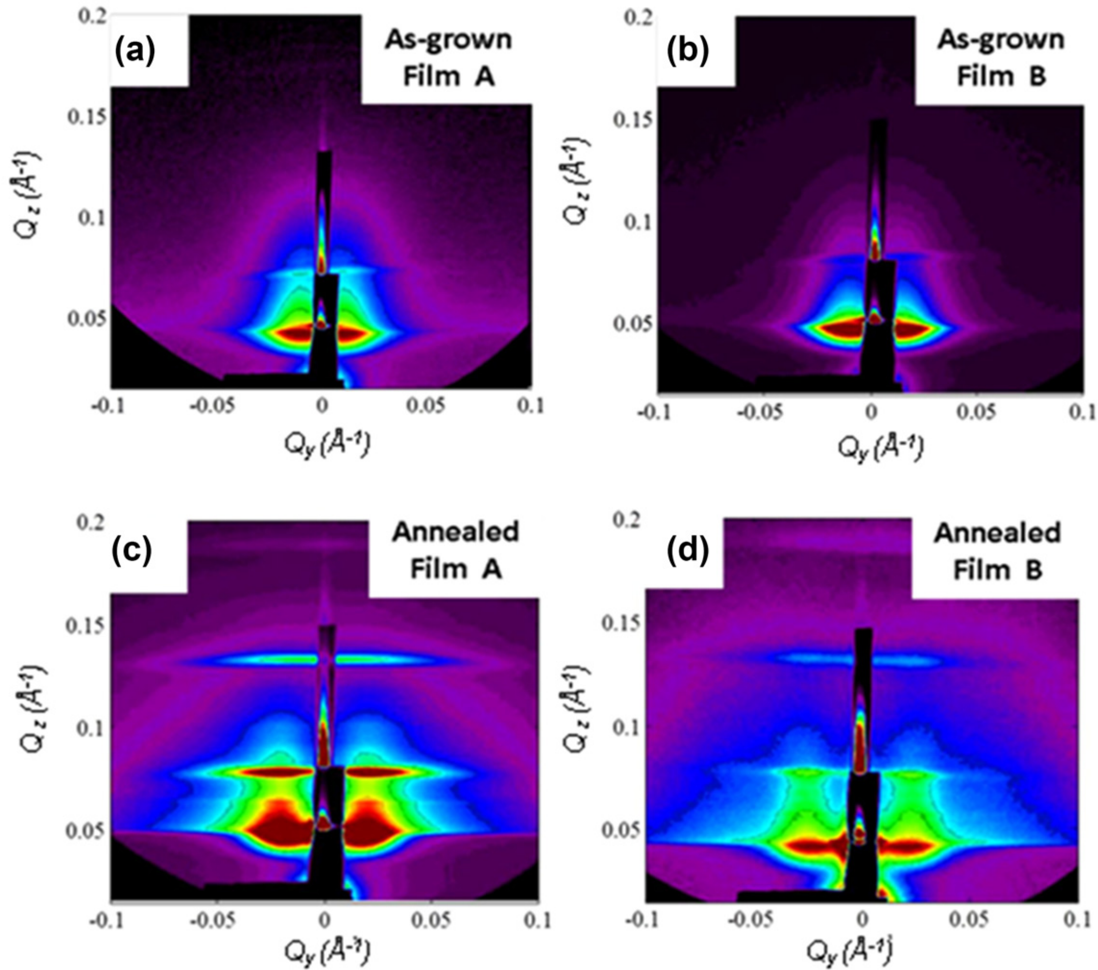

Figure 3. GISAXS intensity distributions of the as-grown (*a*), (*b*) and annealed (*c*), (*d*) films A and B for a grazing incidence angle of 0.35°.

they correspond to the multi-layer structure. A characteristic feature from the sample surface dominates in the central part of the GISAXS maps ($Q_y \sim 0$), whereas no GISAXS intensity is observed at larger Q_y-values indicating the absence of cluster formation during deposition (i.e. a nearly homogeneous mixture of alumina, Ge and Si atoms occurs). On the other hand, GISAXS images of the annealed films show strong lateral correlation maxima in addition to Bragg sheets. The semi-circular feature in the background shows the formation of nearly spherical clusters in the films after annealing. The lateral maxima show the existence of nano-objects that have strong correlation in their in-plane positions.

In order to investigate the cause of these lateral maxima, GISAXS maps from the as-grown and annealed film B were obtained at an incidence angle equal (figure 4(*a*)) and slightly greater than the critical angle (figure 4(*b*)), so that the whole depth of the films was probed. In particular, the GISAXS map obtained at an incidence angle equal to (or slightly less than) the critical angle indicates nicely ordered surface morphology features. These features are visible in the cross-sections of the films (see figure 2(*b*)). The period of the surface features is found to be 28 nm from the analysis of GISAXS maps [16]. The calculated period is significantly larger than the average separation of NCs measured by HAADF-STEM analysis (see figure 2). An absence of vertical sheets (which are usually a consequence of the multi-layer structure) in this GISAXS map proves that the probing depth is indeed very shallow (i.e. only the surface layer is observed). An increase of the incidence angle and slightly greater than the critical angle (figure 4(*b*)) causes the appearance of vertical sheets, while maintaining the lateral features with approximately the same or lower intensity compared with the case of a shallow measurement. This fact shows that the lateral ordering that is visible in the GISAXS maps actually comes from the surface of the film. Stress in the film might have some influence and a more detailed study about this surface effect on the organization of these structures is needed and will be done in a further work. The contribution from the surface region is very high and it is superimposed on the NCs' contribution; therefore, it is impossible to determine precisely the sizes of the NCs and their arrangements within the films. However, the strong semi-circular background in the GISAXS maps measured with higher incidence angle clearly shows the presence of approximately spherical nanoclusters in the films. Additionally, the GISAXS maps do not display lateral features that would indicate correlation in lateral (within the layer) nanocluster positions. The multi-layer period is determined to be 10.0 ± 0.5 nm.

The internal properties of as-grown and annealed films were studied by XRR (figure 5) in order to find out about layer thickness and interface roughness [27]. Furthermore, the

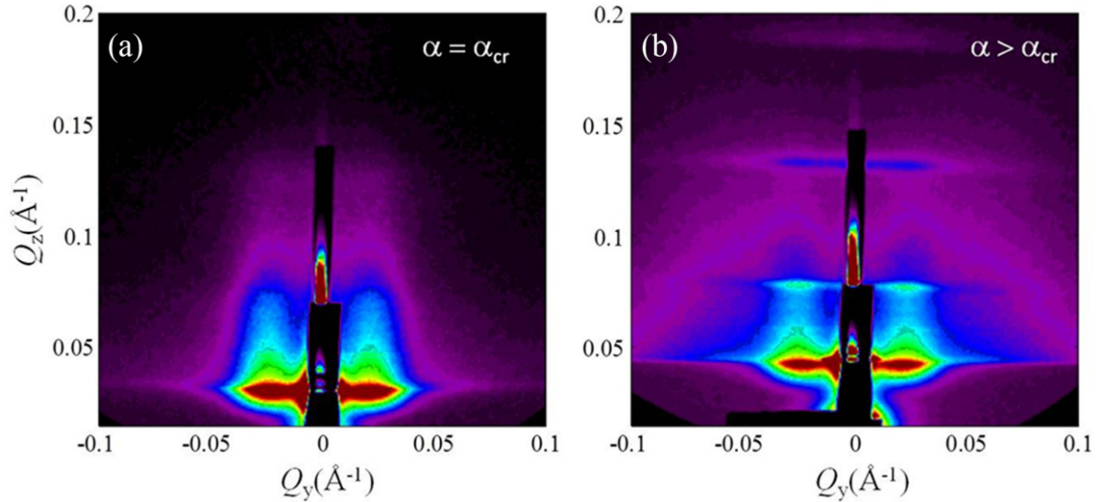

Figure 4. GISAXS maps of annealed film B for incidence angles equal to and slightly greater than the critical angle, respectively: (*a*) $\alpha_{cr} = 0.30°$ and (*b*) $\alpha = 0.35°$ ($> \alpha_{cr}$).

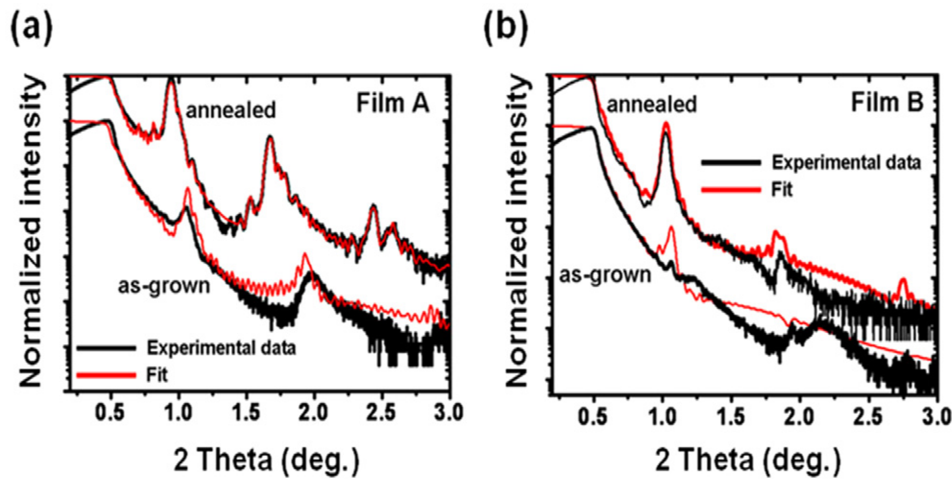

Figure 5. XRR curves of as-grown and annealed film A (*a*) and B (*b*). The corresponding fits are shown as red solid lines. Curves have been vertically shifted for clarity. Distinct differences in the multi-layer peaks are caused by variations in layer properties.

XRR technique can provide statistical information averaged over a large sample area. Satellite maxima corresponding to the multi-layer periodicity can be observed for the samples at $\theta = \theta_m$ ($m = 1, 2, 3$, etc) showing that the samples consist of alternating Al_2O_3 and SiGe/Al_2O_3 layers with a vertical period Λ_{XRR}. From figures 5(*a*) and (*b*), it can be seen that the reflectivity of the as-grown films differs significantly from that of the annealed films. In general, film A presents well defined XRR peaks due to a better interface quality between SiGe NCs and Al_2O_3 layers, in agreement with STEM measurements. Interestingly, the annealing process improves the resolution of the observed peaks indicating a lower structural disorder at the interfaces. The annealed sample B exhibits higher interfacial roughness compared to the annealed sample A. The as-grown and annealed films A exhibit a Λ_{XRR} value of 9.3 nm (SiGe+Al_2O_3 = 3.3 nm, Al_2O_3 = 6 nm) and 10 nm (SiGe+Al_2O_3 = 3.5 nm, Al_2O_3 = 6.5 nm), respectively. The as-grown and annealed films B present Λ_{XRR} values of 9.5 nm (SiGe+Al_2O_3 = 4.0 nm, Al_2O_3 = 5.5 nm) and 10 nm (SiGe+Al_2O_3 = 4.1 nm, Al_2O_3 = 5.9 nm), respectively. These results are in agreement with STEM observations. The best fits to the experimental data were obtained using the Parratt's formalism [28]. The theoretical curves were adjusted using a generic algorithm and the Levenberg–Marquardt methods. The observed discrepancies between theoretical and experimental curves (peaks positions) are mainly due to small variations in the layer thickness and roughness along the multi-layer. A rough estimation of the interface roughness from about 0.5 nm to 1.5 nm is obtained for both films A and B, being the lower limit corresponding to as-grown films.

3.2. *Structural properties of the films: Layer composition*

The composition of the multi-layer structure was studied by EELS. Al-$L_{2,3}$ and O-K edges in the EELS spectra are associated with Al_2O_3 regions, which appear darker in HAADF images. By removing the background under the EELS spectra using a power law fit and integrating the remaining intensity under the different edges, we obtain element sensitive maps associated with the area indicated in figures 6(*a*) and (*d*). The Al and O maps are shown in greyscale

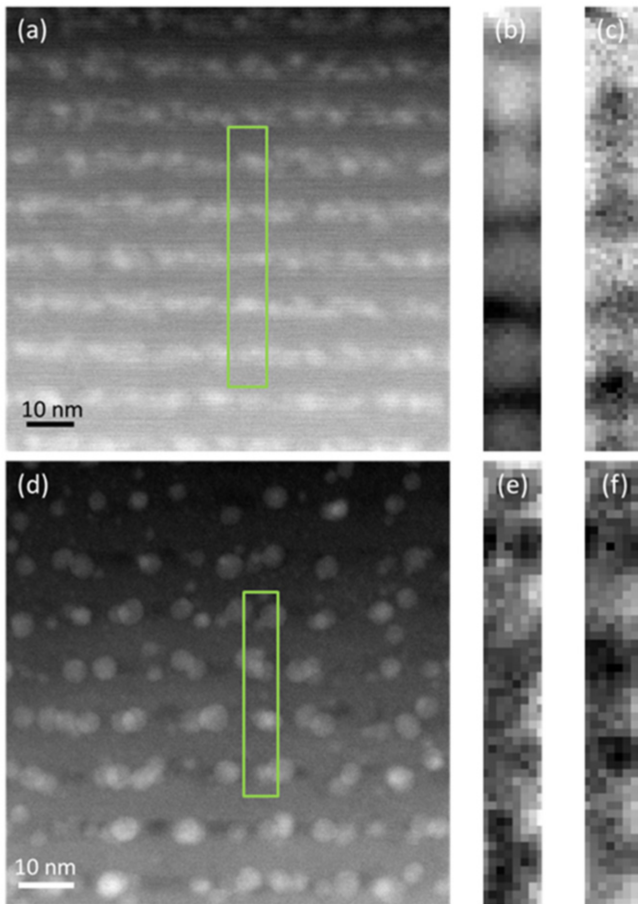

Figure 6. HAADF-STEM images of the films A (*a*) and B (*d*). The green rectangle shows the specific region where an EEL spectrum image was acquired. Greyscale Al-$L_{2,3}$ map (*b*) from (*a*), (*e*) from (*d*) and O-K map (*c*) from (*a*), (*f*) from (*d*). All maps were produced after background subtraction using a power law fit.

in figures 6(*b*),(*c*) and (*e*),(*f*) for annealed films A and B, respectively. For the two annealed films, we can see clearly that the contents of oxygen and aluminum are lower inside the SiGe NC layers than in the Al_2O_3 layers. Thus, ultra-thin Al_2O_3 separation layers act as efficient barriers to confine the SiGe NCs within their lateral formations. Interestingly, SiGe NCs touching each other in the layers (film A) and isolated SiGe NCs (film B) are well resolved in the images.

Figure 7 shows RBS spectra obtained for as-grown film B. At a 70° tilt angle (20° incidence of the beam with the surface of the sample, and 18.7° exit angle), the entire stack is probed so the total thickness can be determined, as well as the amounts of Ge, Al, and O. The data was analysed with the code NDF [29]. The model used in the fits [30] assumes SiGe spherical NCs distributed in layers in the Al_2O_3 matrix, where the average size and the Ge fraction x in the NCs was estimated from STEM measurements, and the amount of Si is indirectly inferred from the amount of Ge present. At an 82° tilt angle (8° incidence and 7.5° exit), the depth resolution at the surface is around 3 nm for the Ge signal, and given that the period is around 10 nm, separate Ge peaks should be possible to observe. The main difficulty is the very small total amount of Ge in each layer containing NCs, leading to poor statistics in the RBS data. Nevertheless, as can be seen in the inset of figure 7(*b*), indeed the first few Ge peaks are observed. At greater depths, the depth resolution degrades due to energy straggling of the beam, and the fits were done simply assuming that there is no strong degradation of the multi-layer quality deeper in the sample. The slightly larger size of the NCs observed with STEM close to the Si substrate was introduced in the fitting model.

Figure 8 shows depth concentration profiles of as-grown and annealed films obtained from the fits to the experimental RBS intensity distributions. The profiles show the existence of Si, Ge, Al and O. In addition, a low concentration of residual Ar atoms (not shown) from the sputtering process was also detected in both as-grown and annealed films. Si and Ge atoms are localized within the layers before and after the annealing process, in agreement with STEM, GISAXS and XRR measurements, thus indicating a well-organized multi-layer structure. The estimated average bi-layer thicknesses were found from RBS fittings to be $\Lambda_{RBS} = 9 \pm 1$ nm and $\Lambda_{RBS} = 8 \pm 1$ nm for as-grown films A and B, respectively. Similar values were obtained for the annealed films. These values are in relatively good agreement with the STEM results. The Si : Ge ratios found in films A and B before annealing are 1 : 2. Surprisingly, a significant loss (but less than half) of the amount of Ge is evidenced in the film B after the annealing. This suggests some Ge out-diffusion from the film possibly due to formation of volatile GeO_x species for the annealing procedure used. This has already been observed for Ge+Al_2O_3 films [31]. We attribute the enhanced diffusion process in film B after annealing to a possible fluctuation in the in-plane morphology of the layer where some degree of clustering could have occurred during the first stages of the deposition of the Si and Ge atoms, due to their relative large mobility in comparison with these species in film A. Hence, a less compact layer is formed increasing the contact area of the rough SiGe layer to oxygen from the surrounding Al_2O_3 matrix layer.

3.3. PL properties

Figure 9(*a*) shows room-temperature PL spectra of as-grown and annealed (at 700 and 800 °C) film A in the photon energy range 1.8–3.2 eV. All films show broad PL in the whole region of measurement. For a better understanding of the PL data, the spectra have been normalized and deconvoluted using Gaussian functions as shown in figure 9(*b*). Specifically, the PL spectra for film A have been decomposed into two peaks centred at: 2.50 eV (full-width at half-maximum (FWHM) = 0.63 eV) and 2.86 eV (FWHM = 0.43 eV) for the as-grown film; 2.60 eV (FWHM = 0.63 eV) and 3.10 eV (FWHM = 0.43) for the annealed (at 700 °C) film; 2.72 eV (FWHM = 0.67 eV) and 2.96 eV (FWHM = 0.37 eV) for the annealed (at 800 °C) film. Hence, no appreciable shift in the PL energy peak is observed as a function of the annealing temperature. Furthermore, a similar PL response is measured for film B (see inset to figure 9). Considering the NCs size range of 3–5 nm in annealed films A and B, and taking into account that NCs are Ge-rich, theoretical calculation assuming confined exciton recombination in the NCs predicts a variation

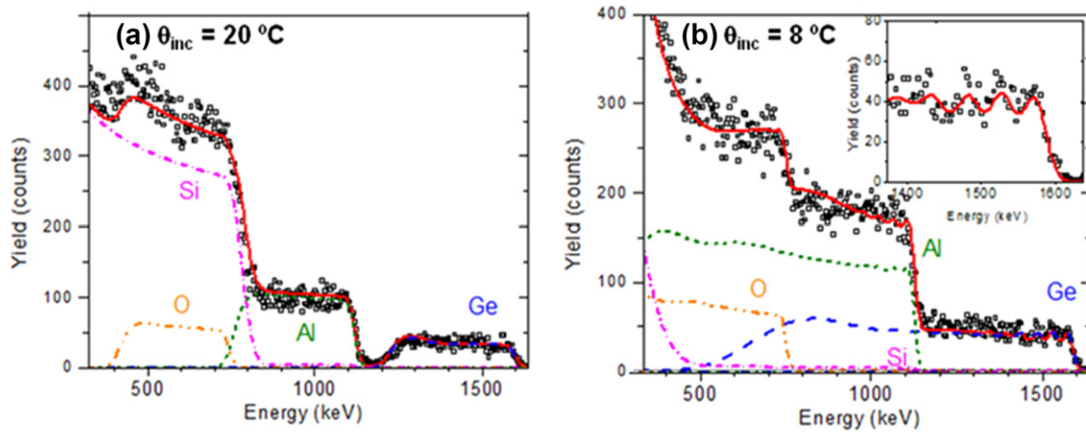

Figure 7. RBS spectra obtained for the as-grown films B, at (*a*) 20° and (*b*) 8° angle of incidence with respect to the surface of the sample. The inset in (*b*) shows the Ge signal. The fitted partial signals of each element are also shown.

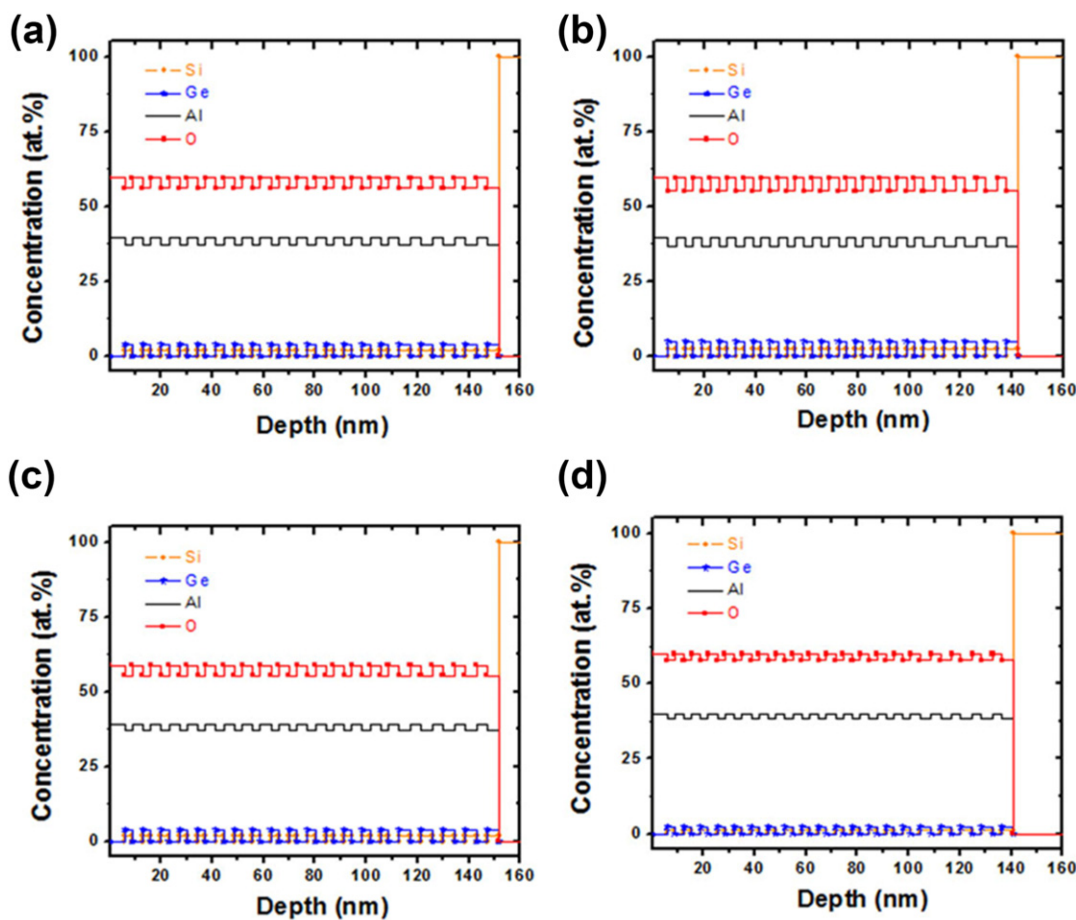

Figure 8. Concentration depth profiles (derived from RBS measurements) for different elements (Si, Ge, Al, O and Ar) present in the as-grown ((*a*) and (*b*)) and annealed ((*c*) and (*d*)) films A and B, respectively.

of the exciton energy in the range from 0.75 to 1.60 eV [32]. However, the energy position of the PL peaks obtained for films A and B is clearly larger than that expected assuming radiative recombination of quantum-confined excitons in the $Si_{1-x}Ge_x$ NCs. Size-independent PL of Ge NCs in the energy range of 2.5 to 3.2 eV has been attributed to oxygen vacancies, oxygen–germanium vacancy pairs, and related defect centres [20–22]. The reference annealed Al_2O_3 matrix at 800 °C does not present PL emission in this wavelength range (not shown here). Hence, we suggest that the origin of the blue-PL band is not due to radiative recombination of quantum-confined excitons in NCs or defect centres in the Al_2O_3 matrix, but are more likely to be due to $Si_{1-x}Ge_x$/O defects that could be related with the interface between the NCs and the matrix material. Moreover, it is observed that the PL intensity for film A increases significantly after performing an annealing at 700 °C due to NCs formation in the matrix (i.e. formation of interface related defects). However, this PL decreases with

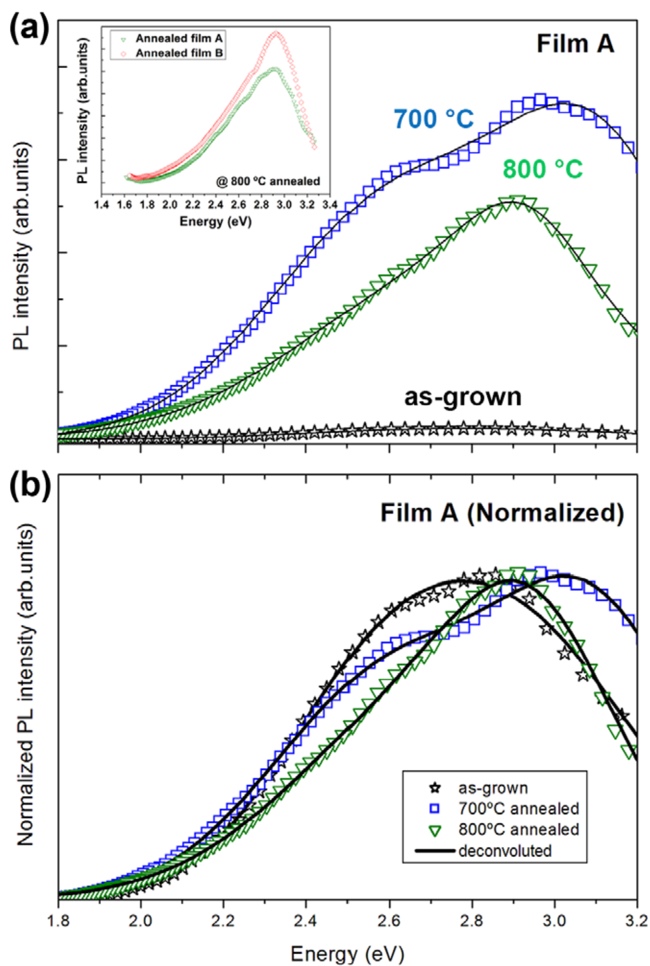

Figure 9. RT PL spectra of as-grown and annealed (at 700 and 800 °C) films produced at 60 W RF-power (film A) in the photon energy range 1.8–3.2 eV (*a*) and normalized PL curves (*b*). The inset shows the PL spectrum of the films A and B annealed at 800 °C.

the annealing temperature (from 700 to 800 °C). We attribute it to the partial removal of defects in the NCs interface with the matrix. The low intensity PL observed for the as-grown film is attributed to interfacial defects of the amorphous layers with the surrounding matrix.

4. Conclusions

The structural and compositional properties of $SiGe/Al_2O_3$ multi-layer structures grown at RT are investigated for 60 W and 80 W RF-power. Annealed multi-layer films produced at relatively high RF-power (film B) show nearly spherical NCs with better discrete and uniform sizes than for annealed films produced at the lower RF-power (film A). Raman and high-resolution STEM measurements confirm the formation of SiGe NCs in well confined 2D layers in annealed films, in agreement with GISAXS measurements. The interface roughness of the layers was studied by XRR and STEM, and showed a larger roughness for film B. PL properties have been investigated and optical emission in the blue energy range 2.0–3.0 eV was measured on both films A and B.

Acknowledgments

This study has been partially funded by: (i) ELETTRA Synchrotron Radiation Center for the measurements at the SAXS beamline; (ii) FEDER through the COMPETE Programme and by the Portuguese Foundation for Science and Technology (FCT) in the framework of the Strategic Project PEst-C/FIS/UI607/2011 and PEst-C/CTM/LA0025/2011; (iii) European COST Actions MP0901-NanoTP and MP0903-NanoAlloy. This work has been supported by the European Community as an Integrating Activity 'Support of Public and Industrial Research Using Ion Beam Technology (SPIRIT)' under EC contract no. 227012. Electron microscopy work at ORNL was supported by the Office of Basic Energy Sciences, Division of Materials Sciences and Engineering, US Department of Energy (SJP, MV). MB acknowledges support from the Croatian Ministry of Science, Higher Education and Sport, (project number 098-0982886-2895). AGR thanks the support of the Karlsruhe Nano Micro Facility (KNMF, www.kit.edu/knmf), a Helmholtz Research Infrastructure at Karlsruhe Institute of Technology (KIT, www.kit.edu). EMFV is grateful for financial support through the FCT and POPH grant SFRH/BD/45410/2008. JMS is grateful for financial support through the Spanish CSIC JAE-DOC-070/01 programme co-funded by FSE. SIM acknowledges support by the Spanish MICINN/MEC (projects TEC2011-29120-C05-03 and CONSOLIDER INGENIO CSD2009-00013) and the Junta de Andalucía (PAI research group TEP-120; project P08-TEP-03516). MR acknowledges financial support from the European Research Council Starting Investigator Award 'STEMOX'. The authors would like to thank Professor David J Barber (University of Essex) for his helpful discussions and critical reading of this manuscript, and Engineer José Santos for technical support at Thin Film Laboratory.

References

[1] Hong S, Kim M, Jeong P, Choi S-H and Kim K 2008 *Nanotechnology* **19** 305203
[2] Buljan M, Desnica U V, Dražić G, Ivanda M, Radić N, Dubček P, Salamon K, Bernstorff S and Holý V 2009 *Nanotechnology* **20** 085612
[3] Rodríguez A, Rodríguez T, Prieto A, Jiménez J, Kling A, Ballesteros C and Sangrador J 2010 *J. Electron. Mater.* **39** 1194
[4] Pinto S R C *et al* 2010 *Microelectron. Eng.* **87** 2508
[5] So Y-H, Huang S, Conibeer G and Green M 2011 *Thin Solid Films* **519** 5408
[6] Zschintzsch M, Borany J von, Jeutter N M and Mücklich A 2011 *Nanotechnology* **22** 465302
[7] Gardelis S, Nassiopoulou A G, Manousiadis P, Milita S, Gkanatsiou A, Frangis N and Lioutas Ch B 2012 *J. Appl. Phys.* **111** 083536
[8] Martín-Sánchez J, Chahboun A, Gomes M J M, Rolo A G, Pivac B and Capan I 2012 *Phys. Status Solidi RRL* **6** 223
[9] Sharma M, Sanyal M K, Mukhopadhyay M K, Bera M K, Saha B and Chakraborty P 2011 *J. Appl. Phys.* **110** 102204
[10] Vieira E M F *et al* 2012 *J. Appl. Phys.* **111** 104323
[11] Buljan M, Bogdanović-Radović I, Karlušić M, Desnica U V, Dražić G, Radić N, Dubček P, Salamon K, Bernstorff S and Holý V 2009 *Appl. Phys. Lett.* **95** 063104
[12] Kanoun M, Busseret C, Poncet A, Souifi A, Baron T and Gautier E 2006 *Solid-Sate Electron.* **50** 1310

[13] Céspedes E, Babonneau D, Lyon O, Sánchez-Marcos J, Rouzière S, Prieto C, Olivi L and Traverse A 2010 *J. Appl. Phys.* **107** 104306
[14] Pinto S R C, Rolo A G, Buljan M, Chahboun A, Bernstorff S, Barradas N P, Alves E, Kashtiban R J, Bangert U and Gomes M J M 2011 *Nanoscale Res. Lett.* **6** 341
[15] Lee J J, Wang X G, Bai W P, Lu N and Kwong D-L 2003 *IEEE Trans. Electron Devices* **50** 2067
[16] Buljan M, Radić N, Bernstorff S, Dražić G, Bogdanović-Radović I and Holỳ V 2012 *Acta Cryst.* A **68** 124
[17] Maeda Y 1995 *Phys. Rev.* B **51** 1658
[18] Takeoka S, Fujii M, Hayashi S and Yamamoto K 1998 *Phys. Rev.* B **58** 7921
[19] Das S, Das K, Singha R K, Dhar A and Ray S K 2007 *Appl. Phys. Lett.* **91** 233118
[20] Min K S, Shcheglov K V, Yang C M, Atwater A, Brongersma M L and Polman A 1996 *Appl. Phys. Lett.* **68** 2511
[21] Zacharias M and Fauchet P M 1997 *Appl. Phys. Lett.* **71** 380
[22] Das S, Singha R K, Gangopadhyay S, Dhar A and Ray S K 2010 *J. Appl. Phys.* **108** 053510
[23] Tsang J C, Mooney P M, Dacol F and Chu J O 1994 *J. Appl. Phys.* **75** 8098
[24] Mooney P M, Dacol F H, Tsang J C and Chu J O 1993 *Appl. Phys. Lett.* **62** 2069
[25] Pezzoli F *et al* 2008 *Mater. Sci. Semicond. Process.* **11** 279
[26] Vernon S P, Stearns D G, Rosen R S 1993 *Appl. Opt.* **32** 6969
[27] Bellet D *et al* 2007 Third generation photovoltaics multilayers investigated by x-ray reflectivity *Proc. 22nd European PV SEC (Milan, Italy)* pp 472
[28] Stoev K and Sakurai K 1997 *Rigaku J.* **14** (2) 22
[29] Barradas N P and Jeynes C 2008 *Nucl. Instrum. Methods Phys. Res.* B **266** 1875
[30] Barradas N P 2007 *Nucl. Instrum. Methods Phys. Res.* B **261** 435
[31] Pinto S R C *et al* 2012 *Nanotechnology* **23** 405605
[32] Barbagiovanni E G, Lockwood D J, Simpson P J and Goncharova L V 2012 *J. Appl. Phys.* **111** 034307